Available online at www.sciencedirect.com
SCIENCE DIRECT®
Journal of Power Sources 129 (2004) 238–245
JOURNAL OF POWER SOURCES
www.elsevier.com/locate/jpowsour

In situ neutron imaging technique for evaluation of water management systems in operating PEM fuel cells☆

R. Satija[a,1], D.L. Jacobson[b,*], M. Arif[b], S.A. Werner[c]

[a] *Montgomery Blair High School, Silver Spring, MD 20901, USA*
[b] *National Institute of Standards and Technology, Gaithersburg, MD 20899, USA*
[c] *University of Missouri-Columbia, Columbia, MO 65211, USA*

Received 23 October 2003; accepted 18 November 2003

Abstract

This paper explores the method of neutron imaging as an experimental tool to perform in situ non-destructive analysis on an operating polymer electrolyte membrane hydrogen fuel cell. Neutrons are ideal for the imaging of hydrogen fuel cells because of their sensitivity to hydrogen-containing compounds such as water. This research focused on using imaging techniques to develop methods for testing and evaluating the water management system of a fuel cell. A real-time radiography dataset consisting of 1000 images at 2-s intervals was used to create a movie which showed water production, transport, and removal throughout the cell. This dataset was also analyzed to quantify and calculate the amount of water present in the cell at any time and masking techniques were used to differentiate between water in the cell flow channels and in the gas diffusion layer. Additionally, a tomography dataset allowed for the creation of a digital 3-dimensional (3-D) reconstruction of the dry cell which can be analyzed for structural defects.

Keywords: Fuel cell; Neutron; Radiography; Imaging; Water management

1. Introduction

The proton exchange membrane fuel cell (PEMFC) is a particularly promising replacement for conventional power sources because it exhibits efficient energy conversion without the chemical pollution associated with fuel combustion. The cell has an operating temperature near 80 °C, removing the need for thermal shielding and allowing for instant startup. Additionally, the direct conversion of chemical energy to electrical energy side steps the inefficient intermediate conversion to heat and can thus result in efficiencies as high as 90%. As a result, the PEMFC has promising applications in transportation and consumer electronics and a considerable amount of research funding is being directed towards improving the efficiency, reliability, and cost effectiveness of a PEMFC system [1]. To aid in this analysis, a neutron imaging test setup was developed and constructed at the National Institute of Standards and Technology (NIST) Center for Neutron Research (NCNR). This research used neutron imaging as a tool for non-destructive analysis of an operating fuel cell, and allowed for analysis of internal cell processes, specifically, the formation and transportation of water throughout the cell.

Efficient water management has become increasingly important in the effort to optimize fuel cell energy production [2,3]. Water is produced as a byproduct in the conversion of hydrogen fuel to electrical energy and exists mostly in liquid form as a result of the low PEMFC operating temperature. Because the proton conductivity of the membrane is highly dependent upon its internal water content, the cell must balance water production and removal to create an equilibrium where the polymer electrolyte membrane is highly saturated without flooding either of the electrodes. A deficiency of water in the flow channels can potentially dry out the membrane, reducing conductivity and efficiency. However, flooding the channels with water impedes gas flow and also reduces efficiency.

In order to evaluate the effectiveness of water management schemes, a method capable of looking inside an operational fuel cell and visualize movement of water dynamics could be very useful. Many non-destructive imaging systems

☆ Supplementary data associated with this article can be found at doi:10.1016/j.jpowsour.2003.11.068.

* Corresponding author. Tel.: +1-301-975-6207; fax: +1-301-926-1604.
E-mail addresses: jacobson@nist.gov, david.jacobson@nist.gov (D.L. Jacobson).
[1] Present address: Duke University, Durham, NC 27708, USA.

0378-7753/$ – see front matter © 2004 Elsevier B.V. All rights reserved.
doi:10.1016/j.jpowsour.2003.11.068

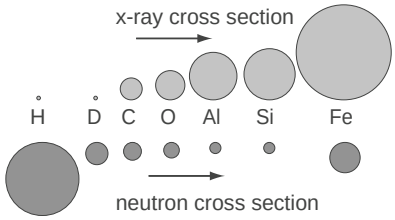

Fig. 1. Comparison of the relative cross-sections of various elements for X-rays and for neutrons.

rely on X-ray radiation, but the X-ray contrast mechanism makes X-ray imaging impractical for the PEMFC. The reason for this is illustrated in Fig. 1. In Fig. 1, we see a visual comparison of relative cross-sections for X-rays and for neutrons. For a constant energy, X-ray attenuation from an element increases with the element's atomic number, resulting in low contrast between lighter elements and the background. Thus, X-ray imaging does not provide sufficient contrast for either hydrogen or water. This lack of contrast makes operational imaging impractical, since one cannot observe the substances flowing through the PEMFC. On the other hand, there exists no correlation between slow or cold neutron attenuation and atomic number. In fact, cold neutrons are heavily attenuated by hydrogen but easily pass through heavier elements such as aluminum. Therefore, neutrons provide the contrast necessary to image the hydrogen and water in a PEMFC without suffering significant reduction while passing through the cell's aluminum encasement. The use of neutrons to image fuel cells was first demonstrated in 1998, when Bellows et al. imaged a PEMFC membrane to determine its water distribution [4].

In addition to imaging in 2-dimensions (2-D), 3-dimensional (3-D) non-destructive analysis using the method of neutron tomography can be performed on an inactive PEMFC to examine inner areas of the cell in 3-D. The computed tomography (CT) data was analyzed using the filtered back projection algorithm (FBPA), which enables accurate 2-D reconstructions of sample cross-sections [5]. The third dimension is obtained by stacking the 2-D slices. This 3-D dataset can be segmented to isolate and observe objects either too small or too attenuating to be observed in an individual radiograph. CT scans are often used in medicine to create a 3-D perspective of bones and tissue.

2. Experimental procedures

The cell used in the experiment was a H-Power Fuel Cell Edu-kit[2] consisting of a four-cell PEMFC stack capable of producing up to 5 A of total current. The original fuel cell had fiberglass endplates which were replaced in house with aluminum since fiberglass contains too much hydrogenous material, thereby reducing the image contrast. Aluminum has a considerably smaller cross-section and is sufficiently rigid to provide enough pressure to allow the cell to work properly. At the top and bottom of the stack there is a current collector plate which is electrically connected to an external load consisting of a rheostat. A schematic view of this stack is shown in Fig. 2. Each cell in the stack consists of hydrogen and oxygen channels, two gas diffusion layers, and one proton exchange membrane (PEM) coated on both sides with a carbon supported platinum catalyst electrode layer.

The neutron images or radiographs described here are shadow images of the neutron beam resulting from attenuation of the neutrons that pass through an object. Neutron beams with large and nearly uniform areas of illumination can be produced by placing a sample a long distance away from a neutron point source, approximated by a circular aperture with a small diameter.

For a neutron beam incident perpendicular onto a 2-D planar slab of material of finite thickness, t, the number of neutrons that make it through the slab in the forward direction is given by,

$$I = I_0 \, \mathrm{e}^{-N\sigma t} \tag{1}$$

where I is the transmitted intensity, I_0 is the incident intensity, N is the atom density, and σ is the neutron cross-section. It follows from Eq. (1) that if σ, I_0, and I can be measured, then one can determine the areal density of the material, Nt being studied. If this is water in a fuel cell then one can resolve the areal density of water in the cell (in $\mathrm{g\,cm^{-2}}$). To do this it is necessary to measure the spatial intensity of the attenuated neutron beam with sub-millimeter accuracy.

A neutron-to-light converter screen is used to record a 2-D matrix of neutron intensity values with sub millimeter accuracy. This screen is 20 cm wide × 20 cm tall × 100–500 μm thick and is made of ZnS with ^{6}Li and Cu embedded in the ZnS matrix. Neutrons are strongly absorbed by ^{6}Li and the resulting nuclear reaction produces highly energetic ^{4}He and ^{3}H charged particles that deposit their energy into the ZnS(Cu), which in turn scintillates light in the green spectral region ($\lambda = 530$ nm). This image is captured with an Apogee Instruments AP-6 cooled CCD camera[2] that focuses on this screen through a lens and a 45° mirror. The mirror allows the CCD camera to be placed outside of the main beam, which would destroy the radiation sensitive electronics. To minimize the background light levels the scintillator and camera assembly are shrouded in a light tight box. An illustration of this camera system can be seen in Fig. 3.

In addition to reducing the ambient light background, the effects of thermal noise in the CCD camera is reduced by cooling the CCD chip to −40 °C using a thermoelectric cooler. The heat removed by the cooler is discarded to a circulating water bath maintained at 20 °C. Cooling the CCD camera reduces the effects of the dark current, which is defined as the tendency of a CCD sensor to produce unwanted

[2] Certain trade names and company products are mentioned in the text or identified in illustrations in order to adequately specify the experimental procedure and equipment used. In no case does such identification imply recommendation of endorsement by the National Institute of Standards and Technology, nor does it imply that the products are necessarily the best available for the purpose.

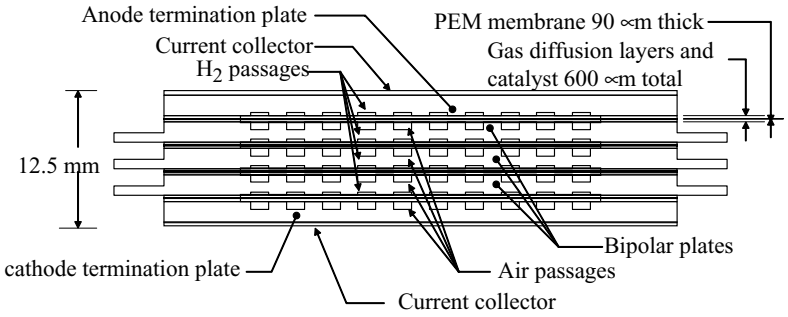

Fig. 2. Cross-sectional view of the fuel cell stack.

charge in each pixel as a function of time. This is a temperature dependent effect caused by thermal electrons gaining enough kinetic energy to tunnel into the wells of the CCD chip. Lowering the system temperature reduces the energy available to these electrons.

The image that is recorded using the CCD camera is a 2-D matrix of count values, $C(i, j)$, where ($0 \leq i \leq 1023, 0 \leq j \leq 1023$). Each pixel represented a 2-D box of 100 μm × 100 μm with a count value ranging from 0 to 16383 (the limit of a 14-bit number). The number of counts is related to the neutron intensity I by an unknown, but constant, efficiency factor, ϵ by the relation $C'(i, j) = C(i, j) - C(i, j)_{\text{dark frame}} = \epsilon I(i, j)$. Here, the much reduced dark current and bias counts, referred to here as the dark frame, have been subtracted from the counts image. However, to avoid having to measure the efficiency factor, the intensity of the empty neutron beam $C'_0(i, j) = \epsilon I_0(i, j)$ was measured so that each dataset could be described by the transmission, $T(i, j)$, given by

$$T(i, j) = \frac{C'(i, j)}{C'_0(i, j)} = \frac{I(i, j)}{I_0(i, j)} = \mathrm{e}^{-N(i,j)\sigma t}. \quad (2)$$

This new matrix is a 1024×1024 matrix of fractional floating point values representing the 2-D transmission of the cell. Eq. (2) can then be inverted to give the areal density

$$N(i, j)t = \frac{-\ln[T(i, j)]}{\sigma}. \quad (3)$$

The experiments were performed at the NCNR on the NG-0 beam line, shown schematically in Fig. 4. The instrument features a special curved guide made of glass coated with a nickel–titanium super mirror, which only reflects cold neutrons. Bending the cold neutrons from the main beam containing gamma rays and fast or high-energy neutrons significantly reduces background radiation [6]. The instrument consists of two beam shutters, both consisting of a ^{6}LiF-polymer of thickness 4.66 mm to stop the cold neutrons, along with a 240 mm thick iron block reducing the dosage of fast neutrons and gamma rays to less than 1 mrem h^{-1}. A series of circular apertures then shaped the beam into a cone with a radius defined by the diameter of the apertures. The neutron fluence of the beam at the 1 cm primary aperture in Fig. 4 is 2.45(5) × 10^9 cm^{-2} s^{-1}.

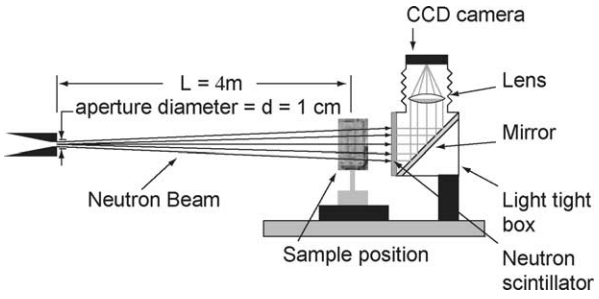

Fig. 3. Experimental setup for imaging of fuel cell. Neutrons were converted to light using a scintillator screen, and the light was focused on the CCD chip.

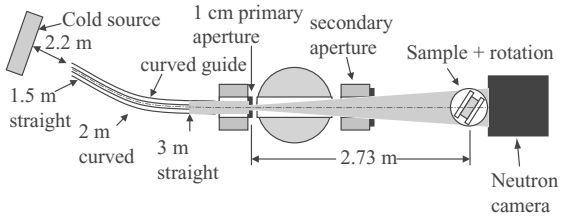

Fig. 4. Diagram of NG-0 Beam Line. The instrument has a curved guide to create a clean beam of thermal neutrons.

3. Experimental design and setup

The experimental setup is designed to detect the neutrons passing through an operational fuel cell as shown in Fig. 3. Here, the PEMFC is placed on a computer-controlled rotation table capable of rotating a sample about the vertical axis. This feature enables the automated collection of tomography data, which requires image acquisition from multiple angles distributed evenly about a 180° rotation.

3.1. Radiography data acquisition

The purpose of neutron radiography experiment is to monitor the fuel cell during operation in order to observe water formation. A series of images of the running cell were taken over a 15 min-period. An exposure time of 1.0 s was chosen to provide a good balance between image quality and

sampling frequency. Each radiograph represents an image looking vertically through the top of the stack, assuming the orientation given in Fig. 2 is the orthogonal horizontal cross-section. While this view does not allow for distinction between various layers of the cell such as the individual four stacks and membranes, it allows for real-time monitoring of water formation in the gas flow channels of the cell.

3.2. Tomography data acquisition

A tomography dataset consists of radiographs of the object from multiple angles evenly spaced about a 180° interval. After each radiograph, the cell is rotated by an interval of 0.4°. Three images are taken and averaged at each angle to minimize the random noise introduced by reading the electronic CCD sensor [5]. A computer automated the operation of rotating the sample, exposing the CCD camera, and saving each image.

3.3. Image processing

Each radiograph undergoes several image processing steps. First, each image is corrected for the dark current and then divided by the dark current correct image of the dry cell (radiography data) or the dark current corrected empty beam image (tomography data). A 3×3 median filter is then applied to the pixels in the images where the pixel value is unusually higher or lower than the values in the surrounding 3×3 neighborhood [5]. This selective median filtering method reduces the loss of image resolution that a global median filter would cause.

4. Data and discussion of results

4.1. Radiography dataset

Individual radiographs are normalized by the images of the empty beam. The images are displayed as grayscale images where white pixels in the image represent areas of highest transmission ($T = 1.0$), and black pixels represent areas of lowest transmission ($T = 0.0$). Intermediate transmission values are then a grayscale mapping of the values between $T = 1.0$ and 0.0. These grayscale images are later processed to produce color images in order to improve the visual dynamic range. Each CCD pixel represents an area of $160\,\mu m \times 160\,\mu m$.

A high-resolution radiograph of the dry, non-operational cell is shown in Fig. 5. The radiograph displays the empty hydrogen gas flow channels (the channels have high neutron transmission), and closer examination reveals the superimposition of the oxygen gas channels, which are located on the opposite side of the membrane.

The radiography dataset consists of 1000 images of the operating cell taken at 1 s intervals with a 1 s image download dead time resulting in a total time delay of 2 s per image. Data collection began when the cell was dry and had just been activated; thus no water appears in the radiographs at time $t = 0$ (see Fig. 6. Water begins to appear as a darker spot (lower transmission) in the cell flow channels as early as 200 s into the dataset. Water appears as a dark spot because the hydrogen in the water heavily attenuates the neutron beam, resulting in low transmission. Separate experiments demonstrated that the radiography was capable of detecting water in quantities less than 1 μg in a pixel area.

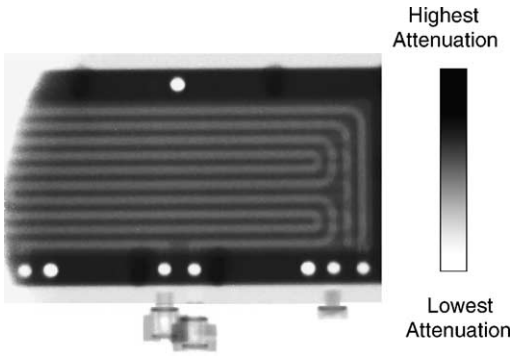

Fig. 5. Neutron radiograph of a dry non-operational fuel cell.

Fig. 6 shows an isolated image in this dataset that reveals significant water formation after 1600 s. However, the real power in this technique lies in the ability to examine all images in sequence as a movie. This movie, described in Appendix A, allows for qualitative visual evaluation of the water management system. The movie clearly shows large amounts of water forming in, travelling through, and exiting the flow channels. The ability to look inside an operational cell and see water forming and moving throughout the cell makes it relatively simple to determine if water is being produced and efficiently removed during operation.

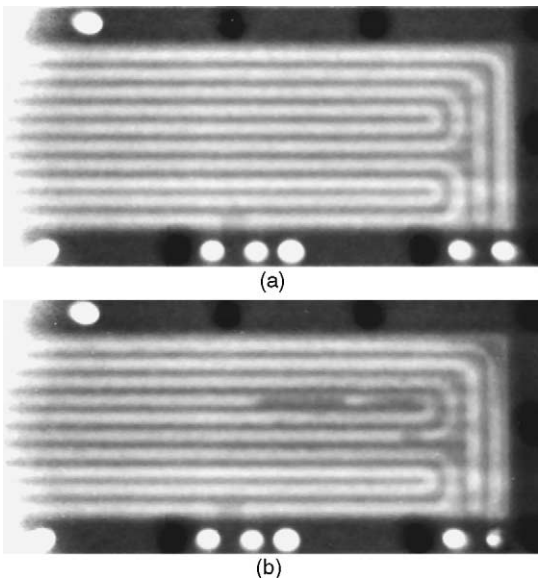

Fig. 6. Neutron images of the fuel cell at 0 s when dry and at 1600 s when water has formed in the channels. Water shows up as a darker region (low transmission) in the flow field region.

The radiography dataset is thoroughly analyzed for information regarding the cell's water management. The first calculation attempted to obtain information about the location of water content in the cell. Water initially forms throughout the gas diffusion layer on the cathode side of the cell where the protons that have passed through the PEM combine with oxygen gas. Most of the water then collects in the oxygen flow channels but some passes through the gas diffusion layer to humidify the membrane or collect in the hydrogen flow channels on the anode side.

To remove the background of the fuel cell components from the image the $t = 0$ dry cell image was divided from all images in the dataset to obtain the transmission due to the water given by

$$T_{\text{water}}(i, j) = \frac{T(i, j)}{T_{\text{dry}}(i, j)} = \mathrm{e}^{-(N\sigma t(\text{water}))}. \quad (4)$$

Dividing out the dry fuel cell image, taking the natural log, and negating the pixel values results in pixel values that correspond to $N\sigma t$, the quantity describing the areal scattering density. In Fig. 7, a colorized time average image of the $N\sigma t$ values for the water distribution in the cell is shown.

Image masking techniques are used to determine the location of water formation in the cell. Image masking refers to the process where all information in an image is lost except for pixels whose location lies within a specified mask region.

Applying masks to any fuel cell image can isolate water formation in the anode channels, the cathode channels, or the gas diffusion layer. Masking analysis was applied to a normalized averaged image, Fig. 7, and the results of the anode and cathode channel masking on the normalized averaged image are shown in Fig. 8a and b. Notice that in the anode-masked image, water is not distributed smoothly throughout the flow channel. Specifically, the curved ends of the hydrogen flow channels have very low water content while regions adjacent to the curves are filled with water. Closer examination of the anode masked image reveal that the areas of highest water density are those which overlap the cathode flow channels while non-overlapping areas have little or no water density. Contrastingly, the cathode-masked image shows no sudden gaps in water density and it is clear that the cathode mask "fits" the water density image very well. These observations imply that most of the water is located on the cathode side of the cell. While there is likely water formation on the anode, it is difficult to differentiate from water on the cathode side since the flow channels have so much overlap. If the hydrogen and oxygen flow channels were completely mutually exclusive, it would be simple to differentiate between water formation on the anode and cathode sides.

The final masking technique attempted to detect water in areas outside of both the hydrogen and oxygen gas channels. This water is spread throughout the gas diffusion media, most likely on the cathode side. The results of this analysis, shown in Fig. 8c, reveal that most of the water is located near the center of the cell while less water density is located in the upper and lower areas. The lack of water content in the gas diffusion media in areas that are horizontally distant from the center of cell may indicate decreased power production in these areas, perhaps as a result of decreased gas flow. However, the lack of water content may also be

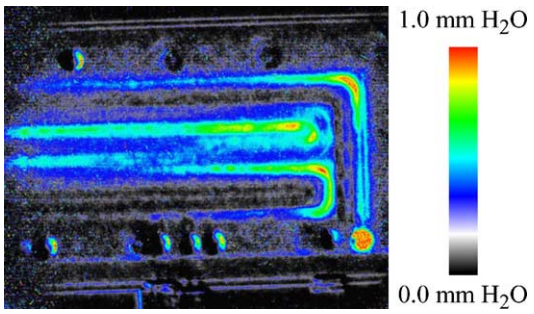

Fig. 7. Image sum of all radiographs. The average water distribution is shown in this figure. The color scale goes from $N\sigma t = 0$ to $N\sigma t = 0.3$, which corresponds to $t = 1.0$ mm of H_2O.

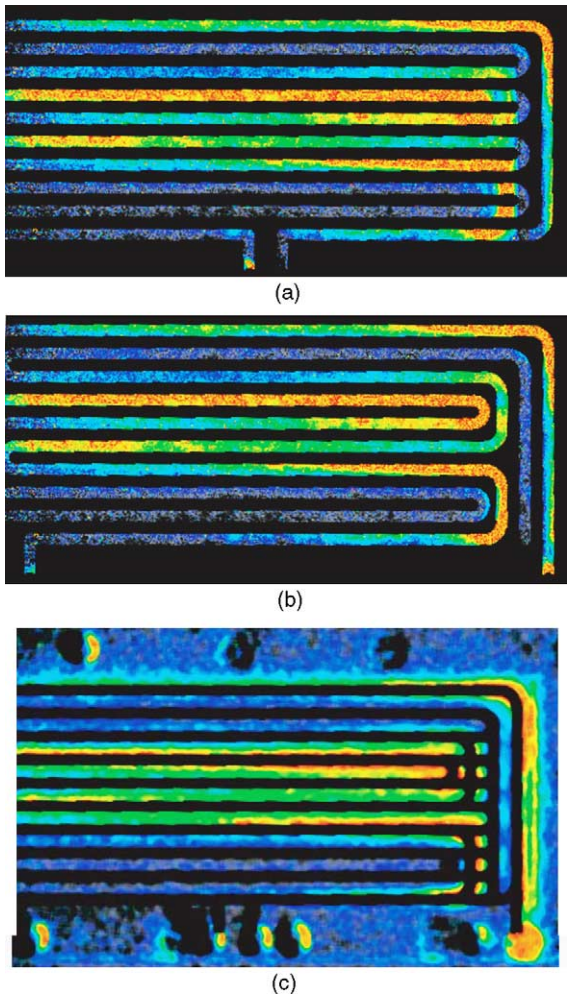

Fig. 8. Image masks applied to summed image (a) anode mask, (b) cathode mask and (c) gas diffusion media (land areas of carbon bipolar plate) mask.

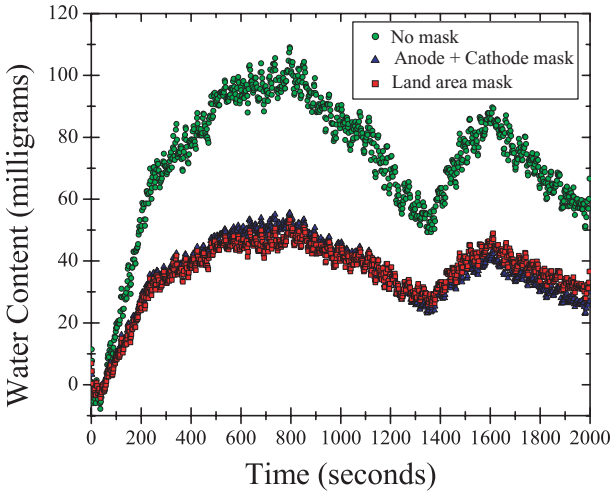

Fig. 9. The total water mass summed over the entire cell with no mask applied plotted along with the sum over the region including both the anode and cathode flow channels and also the land regions of the bipolar plate outside of the anode and cathode flow fields. The land region is gas diffusion media and membrane only.

a result of extremely efficient water management and removal. Either way, the large disparities in water content in different cell locations imply that power production is not uniform throughout the cell which means that the cell is not functioning at maximum efficiency.

Since σ is constant for all water molecules, dividing by σ yields Nt, the areal density of attenuating water atoms in the 2-D pixel area. This density information is easily converted to grams and the total water content can be quantified simply by adding the grams of water in each pixel. The results of this analysis are shown in Fig. 9, a plot of water content in the fuel cell vs. time. The alternating increases and decreases in total water content correspond to periods of water production and water removal in the fuel cell. The results demonstrate that while some water removal takes place, a significant quantity of water remains inside the cell which could impede gas flow in the cell the cell and thus reduce efficiency.

Once the total water content has been calculated, image masking is then be used to approximate how much of the water is located in the two main features of the cell: the gas diffusion media and the flow channels. The similarity between these two series implies that there may be some interaction between the water in these two areas. For example, high water content in the gas diffusion media may condense into the flow channels resulting in higher water content in the channels as well. It is interesting to note, however, that the stack initially contains slightly more water in the channels, but this trend slowly reverses over time.

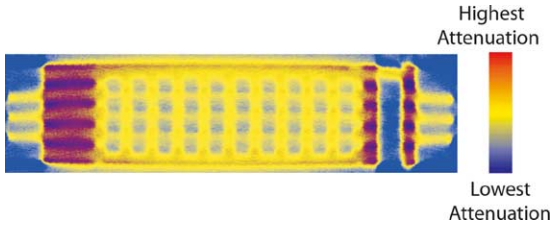

Fig. 10. 2-D vertical slice reconstruction the FBPA was used to create 2-D reconstructions of vertical cross-sections. These reconstructions provide significantly more detail than radiographs of the same area.

4.2. Tomography dataset

The timescale need for acquiring tomography data is of order several minutes to several hours. Therefore, the tomography data is less valuable than radiography data for evaluating dynamic water management systems. However, tomography could be used to identify physical defects in the cell that could impact water management, but could not be used to track dynamic processes inside the cell.

The tomography dataset consisting of 450 radiographs is used to reconstruct vertical slices of the fuel cell and is shown in Fig. 10. The reconstructions are images of scattering cross-section density values, $N\sigma$. In Fig. 11, a drawing of the structure of the PEMFC is superimposed onto the inverted reconstructed slice. The tomographic reconstruction successfully identified almost all of the features present in the PEMFC stack, including all 4 bipolar plates, the separate hydrogen and oxygen air channels, the anode and cathode termination plates, both current collectors, and the gas diffusion and catalyst layers.

The value of tomography, however, lies in the ability to examine a digital, 3-D representation of the cell, as shown in Fig. 12. This stack of images can be sliced or segmented

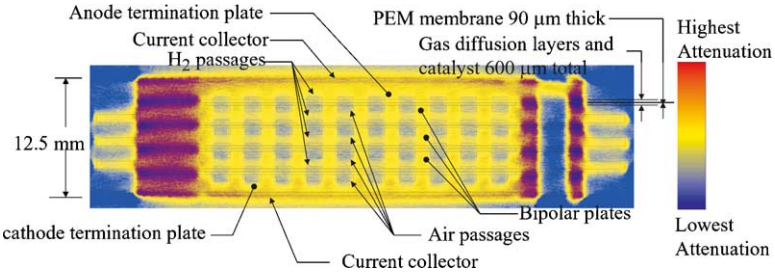

Fig. 11. Structure of PEMFC superimposed onto the slice reconstruction shown in Fig. 10. Tomography was successful in identifying many of the cell's features, yet the system lacked the resolution to distinguish the PEM membrane from the catalyst and diffusion layers.

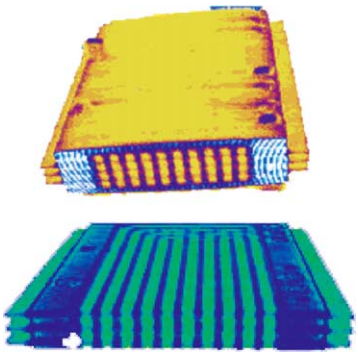

Fig. 12. 3-D reconstructions of PEMFC 3-D views are created by stacking 2-D reconstructions. This 3-D dataset can be "sliced open" to analyze specific features. For example, in the lower image, the fuel cell cover has been removed to reveal the flow channels. Both images are vertically sliced to show inner structure.

in a number of ways to isolate a specific area for inspection. In Fig. 12, visualization software is used to remove the casing and isolate the inner functional parts of the fuel cell. This digital object can be viewed from any angle or zoom level and can be even further sliced to evaluate any part of the fuel cell for damage. Although the benefits of tomography for water-management are limited since real-time monitoring is not currently possible, tomography can be used to search for physical defects in the cell that can affect water management.

5. Conclusions

The ability to image a hydrogen fuel cell using neutron radiation has been demonstrated. As a tool to non-destructively analyze the operational characteristics of a fuel cell, this method is very promising. The test system used here successfully imaged internal features of the cell stack through both real-time radiography and 3-D tomography.

Real-time radiography produces a movie which provides an immediate qualitative evaluation of the water management system. Masking techniques can be used to determine the location of the water in the cell. Normalizing the images allows for quantification of the total cell water content, flow channel water content, and membrane/gas diffusion layer water content. Finally, tomography can be used to create a digital 3-D representation of the cell which can be manipulated to carefully examine any region of the cell for damage. The combination of these techniques allows for a detailed evaluation of the water management system of any fuel cell.

There are a number of improvements to be implemented in future research. Both the time and spatial resolution of the images can be dramatically improved. Faster detectors capable of collecting more light could provide image frames as fast as 0.03 s. This could be achieved with a flat panel amorphous silicon detector that can capture more light and is not as prone to radiation damage as a CCD detector. In principle, a spatial resolution of 100–130 μm is possible with a flat panel detector. This spatial resolution is also near the limit of current commercially available scintillator screens, for which the spatial resolution is of order 100–200 μm.

In order to correlate changes in neutron images with changes in the operational characteristics of the fuel cell, this system should include the capabilities to monitor and record stack voltage, temperature, heat production, and gas flow rate, for each image as it is collected. A more complete facility incorporating these features is currently being incorporated into a new fuel cell imaging station at NIST. The ability to use this station to monitor and evaluate an operating cell can be significantly helpful in the development of an effective water management system. Neutron imaging is a viable topic for future research and could significantly help in improving the efficiency, reliability, and cost effectiveness of the PEMFC system.

Acknowledgements

We would like to thank the NIST Center for Neutron Research for support and use of the neutron facilities during this experiment. We would also like to thank George Lamaze and Heather Chen-Mayer for the use of the NG0beam line. This work was supported by the U.S. Department of Commerce, the NIST Ionizing Radiation Division, NIST Advanced Technology Program, the NIST Center for Neutron Research, the Department of Energy interagency agreement no. DE_AI01-01EE50660, and the National Science Foundation Grant no. PHY-9603559.

Appendix A. Supplementary data

The neutron radiography data gives a 1 s snap shot of the 2-D water distribution in the fuel cell. Each frame of this dataset was taken with a 1 s delay that was required to download data from the CCD sensor. This means that each frame represents the water distribution every 2 s integrated but averaged over 1 s. To show the dynamic information available in this dataset 1000 frames have been linked together to generate a Moving Picture Experts Group (MPEG) movie. The standard playback rate for most MPEG movie decoders is 30 fps and so that was the frame rate chosen for this movie. In the movie, the contrast was adjusted to scale the transmission values from $T = 0.4$ to 0.7. This range optimized the visualization of water, which appears as sections of the images become darker indicating a loss of neutrons due to water scattering. Generally there is water throughout the gas diffusion media and in the flow channels of the bipolar plate assemblies. As the movie develops in time slugs of water develop in the channels and are then pushed out by the gas flow.

References

[1] W. Vielstich, A. Lamm, H. Gasteiger, Handbook of Fuel Cells—Fundamentals, Technology, Application, Wiley, New York, 2003.
[2] T.V. Nguyen, R.E. White, J. Electrochem. Soc. 140 (1993) 2178.
[3] J.S. Yi, T.V. Nguyen, J. Electrochem. Soc. 145 (1998) 1149.
[4] R.J. Bellows, M.Y. Lin, M. Arif, A.K. Thompson, D. Jacobson, J. Electrochem. Soc. 146 (1999) 1099.
[5] A.C. Kak, M. Slaney, Principles of Computerized Tomography, IEEE Press, New York, 1988.
[6] D.F.R. Mildner, H.H. Chen-Mayer, G.P. Lamaze, V.A. Sharov, Characterization of a cold neutron beam from a curved guide, Nuc. Inst. Meth. Phys. Res. A413 (1998) 341.